https://doi.org/10.5194/egusphere-2026-3951
Preprint. Discussion started: 14 July 2026

How exposed is a mountain road to snow avalanches? A corridor-scale assessment in the southern Andes

Iván Latorre[1], Marius Schaefer[2], and Felix Oesterle[3]

[1]Instituto Nacional de Hidráulica, Ministerio de Obras Públicas, Santiago, Chile
[2]Instituto de Ciencias Físicas y Matemáticas, Universidad Austral de Chile, Valdivia, Chile
[3]Department of Natural Hazards, Austrian Research Centre for Forests (BFW), Innsbruck, Austria

Correspondence: Iván Latorre (ivanlatorre@inh.cl)

Abstract. The International Route 115-CH (Pehuenche Pass, ∼36° S, Chile) is a key Andean border crossing that is closed repeatedly each winter by snow and adverse-weather hazard. Yet no calibrated, corridor-scale assessment of avalanche exposure exists for any mountain road in the southern Andes, where systematic avalanche records are largely absent. We combine back-analysis of documented avalanches with corridor-wide simulation in the open-source AvaFrame model (com1DFA). After calibrating friction on two documented paths, we simulate 208 release areas along the 61 km corridor under three snow-depth scenarios. Simulated avalanches reach up to 40 % of the corridor. Of all road crossings, 77 % exceed the 30 kPa vehicle-damage threshold and 41 % exceed the 100 kPa vehicle-destruction threshold, and avalanches typically arrive within a minute of release (median 25 s), leaving little time for evacuation. Mapping these arrival times, the first such analysis for the route, reveals the few segments where preventive closure can substitute for permanent structural protection. Exposure is highly non-uniform: six hot-spot segments, about 7 km (11 %) of the route, concentrate the highest path convergence and define where mitigation would most reduce collective risk. Key limitations are the friction calibration anchored on two documented paths, the 12.5 m terrain model, and the exposure-based framing: results are conditional on avalanche release and do not represent annualized risk. However, using only open-source tools and public data, the workflow is reproducible and transferable to other data-scarce mountain corridors in the Andes and beyond.

1 Introduction

Mountain roads across the Andes are critical arteries for international trade, tourism, and local connectivity between Chile and Argentina. Bilateral trade between the two countries reached approximately USD 8.4 billion in 2024, with most overland freight and passenger traffic channeled through a handful of border crossings that are exposed to snow-related hazards during the austral winter (SUBREI, 2024). Libertadores Pass (3 220 m a.s.l., Ruta 60-CH), the busiest crossing, handled over 2.4 million entries and 479 million kg of goods in 2024, yet closes repeatedly each winter due to snowfall, avalanches, and mass movements. Route 115-CH through Pehuenche Pass (2 560 m a.s.l.) serves as a strategic complement and alternative to Libertadores Pass, connecting the Maule Region in Chile to Mendoza Province, Argentina (Fig. 1). Disruptions on these corridors propagate across supply chains, increase transport costs, and isolate communities that depend on a single surface connection (Wastl et al., 2011; Leone et al., 2014; Oberndorfer et al., 2020); on Canadian highways, avalanche-related traffic delays alone

https://doi.org/10.5194/egusphere-2026-3951
Preprint. Discussion started: 14 July 2026

have been estimated at several million dollars per year (Sinickas et al., 2016). Despite their economic significance, quantitative avalanche exposure assessments for Chilean mountain roads remain scarce.

Snow avalanches threaten mountain roads through direct physical damage, prolonged closures, and vehicle burial; consequences are most severe where the road is the sole surface connection (Wastl et al., 2011; Leone et al., 2014; Oberndorfer et al., 2020). In eastern Canada, for example, avalanche forecasting for the sole road access to coastal communities has driven the development of machine-learning-based warning systems (Gauthier et al., 2025), building on a long national record of avalanche impacts on transportation corridors (Stethem et al., 2003). In the European Alps, quantitative risk frameworks (Wilhelm, 1998; Keylock and Barbolini, 2001; Rheinberger et al., 2009; Eckert et al., 2012) and validated dynamics models (Bartelt et al., 1999; Christen et al., 2010; Sampl and Granig, 2009; Tonnel et al., 2023; Oesterle et al., 2024) enable corridor-scale hazard zoning and protection design (Dalmasso et al., 2025; Ortner et al., 2023; Oberndorfer et al., 2026).

At larger scales, automated hazard indication mapping now covers entire regions: in Switzerland, automated release-area delineation (Bühler et al., 2018) feeds RAMMS simulations that map avalanche hazard for whole cantons under multiple return periods, validated against the avalanche cadastre (Bühler et al., 2022); in Norway, NAKSIN combines climate-dependent release probabilities with automated terrain analysis to produce nationwide susceptibility maps (Issler et al., 2023). A complementary body of work addresses roads specifically. It ranges from the avalanche hazard index for traffic exposure (Schaerer, 1989) to methods for risk evaluation and management of road traffic (Kristensen et al., 2003). Other studies analyze the temporal variability of damage potential on road networks (Zischg et al., 2005) and the operational procedures and information systems that support the winter opening and closure of high alpine pass roads (Margreth et al., 2003; Bründl et al., 2004). These approaches, however, largely rest on the dense observation networks and multi-decadal avalanche cadastres of well-instrumented regions; automated release-area delineation is only beginning to reach data-sparse mountain ranges (Sykes et al., 2022), and no equivalent mapping exists for Andean road corridors.

In the Chilean Andes, comparable tools are largely absent from operational practice. Snow avalanches have caused approximately 400 documented fatalities in central Chile between 1906 and 2001, with 64 % occurring in the mining sector, including the 1944 El Teniente disaster (102 deaths) and the 1984 destruction of the Libertadores Pass border complex (27 deaths) (Ramírez C. and Mery G., 2007). Despite this toll, systematic avalanche observation and control systems remain confined to a handful of mining operations; no public road in Chile currently benefits from the kind of instrumented monitoring and hazard zoning that underpins European road management (Ramírez C. and Mery G., 2007).

The few published avalanche dynamics studies in the Chilean Andes have focused on individual paths or short road segments. Janeras et al. (2013) back-analyzed the catastrophic 1914–1944 Sewell avalanches with Aval-1D and RAMMS, obtaining Voellmy friction values for large historical events. Vera Valero et al. (2016, 2018) modeled wet-snow runout at a high-altitude mine site with RAMMS coupled to SNOWPACK, showing that temperature-dependent friction substantially improves runout prediction for wet flows. Casteller et al. (2018) assessed the role of mountain forests in attenuating avalanche dynamics at Nevados de Chillán, while Casteller et al. (2011) provided the first dendrogeomorphic reconstruction of avalanche frequency in the Patagonian Andes (Lago del Desierto). Vergara et al. (2020) analyzed a century-long record of geo-climatic hazards along Ruta 7 (32–33° S), reporting that mass movements account for the majority of documented events. More recently, Fürst

https://doi.org/10.5194/egusphere-2026-3951
Preprint. Discussion started: 14 July 2026

et al. (2025) revisited the 1987 Parraguirre ice-rock avalanche using r.avaflow, illustrating the potential of open-source numerical frameworks in the Andes. For Route 115-CH specifically, Rauld et al. (2015) documented 168 avalanche paths and Becerra Baeza and de Rurange Espinoza (2018) evaluated mass-movement susceptibility, but neither study included numerical dynamics simulations or a quantitative exposure profile at road level. No corridor-scale avalanche exposure assessment calibrated against large-volume events has been published for a Chilean public road.

We close this gap with a corridor-scale assessment of Route 115-CH. Unlike these site-specific studies, we evaluated the full 61 km corridor using the com1DFA module within the open-source AvaFrame framework (Tonnel et al., 2023; Oesterle et al., 2024), combining back-analysis calibration against large-volume events with corridor-scale extrapolation. We produced: (1) physically calibrated simulations anchored on four documented events across two paths, each providing a calibration/validation pair; (2) an intensity map for 208 release areas covering three return periods (624 simulations); (3) a route-kilometer-resolution exposure and intensity profile directly usable by road managers; and (4) a sensitivity analysis on friction and density parameters (2 496 additional simulations) testing the robustness of the corridor-scale results. Beyond this corridor, the methodological approach (open-source simulation, local calibration from a small number of events, and automated road-level exposure mapping) addresses a general problem: bringing quantitative, corridor-scale exposure assessment to mountain roads in data-scarce regions, where the observation networks and cadastres that support European practice do not exist. Route 115-CH serves as the demonstration case; the workflow is directly transferable to other Andean corridors and comparable settings (Sect. 5.4).

2 Study area

Route 115-CH is located in the Central Andes at approximately 36° S (Maule Region, Chile). The study section extends 61 km from the La Mina sector (900 m a.s.l.) to the Chilean–Argentinian border at Pehuenche Pass (2 560 m a.s.l.), with surrounding catchments reaching 4 000 m a.s.l. (Fig. 1). The route is paved, single-carriageway, and classified as a primary rural road (Class 1, Chilean Ministry of Public Works, MOP). Snow and adverse-weather conditions force recurrent preventive closures each winter, ordered by the regional authority with the closure point set within the modeled corridor (most often near El Médano/La Mina, km 100–104, and Lo Aguirre, km 128–138). Official records (Subsecretaría del Interior, 2026) document 6, 10, and 14 closure orders in 2023, 2024, and 2025, respectively, concentrated between May and September and each in force until conditions allowed. The *Dirección de Vialidad* (MOP) is responsible for the route. ENEL (a power company) operates the Los Cóndores hydroelectric plant between La Mina and Laguna del Maule (∼2 000 m a.s.l.). During the construction phase, the company supported winter road management and snow monitoring through contracted nivology teams. Two sectors concentrate the highest avalanche activity along the corridor (Dirección de Vialidad, 2014, 2021): the *Cuesta Los Cóndores* (km 125–135, 1 400–2 200 m a.s.l.), where avalanches from 14 distinct catchments (paths A31–A45) converge on a narrow road section ascending the main valley, and the *Cuesta La Zorra* (km 154–159, 2 200–2 450 m a.s.l.), a high-altitude sector where persistent snow accumulation is favored by aspect-controlled shading and wind loading. Two previous avalanche studies have been commissioned for the corridor by the *Dirección de Vialidad*: the first (Dirección de Vialidad, 2014) identified more than 150 avalanche paths and classified their susceptibility using a morphometric index. The second (Dirección de Vialidad,

https://doi.org/10.5194/egusphere-2026-3951
Preprint. Discussion started: 14 July 2026

2021) digitized release areas and estimated fracture depths for three return periods ($T = 10$, 30, and 100 yr). It also modeled 29 selected paths with RAMMS (Christen et al., 2010) without formal friction calibration or a corridor-scale exposure profile. Route 115-CH carries approximately 2000 vehicles per day from September to May (MOP, personal communication).

The climate is semi-arid Mediterranean, with precipitation falling predominantly as snow above 1 500 m a.s.l. between June and September. Interannual variability is strongly modulated by ENSO: El Niño years produce enhanced snowfall in central Chile, leading to higher avalanche activity, while La Niña years tend to be drier (McClung, 2013). This teleconnection pattern is similar to that documented for avalanche frequency in the Patagonian Andes by Casteller et al. (2011). The only public weather station in the immediate area is Lo Aguirre (2 000 m a.s.l.), operated by the General Water Directorate (DGA), providing monthly snow density measurements without continuous automatic records. Additional nivological data were obtained from the CARASUR and Viento Puelche nivology teams during the winter operations of ENEL's Los Cóndores hydroelectric project (Viento Puelche, 2018).

The 208 avalanche release areas digitized in this study span elevations of 1 055–3 200 m a.s.l. and aspects ranging from N to SW, reflecting the complex topography of deeply incised east–west tributary valleys. For the *Severe* scenario (Sect. 3.1), estimated release volumes span $\sim$590–535 000 m^3.

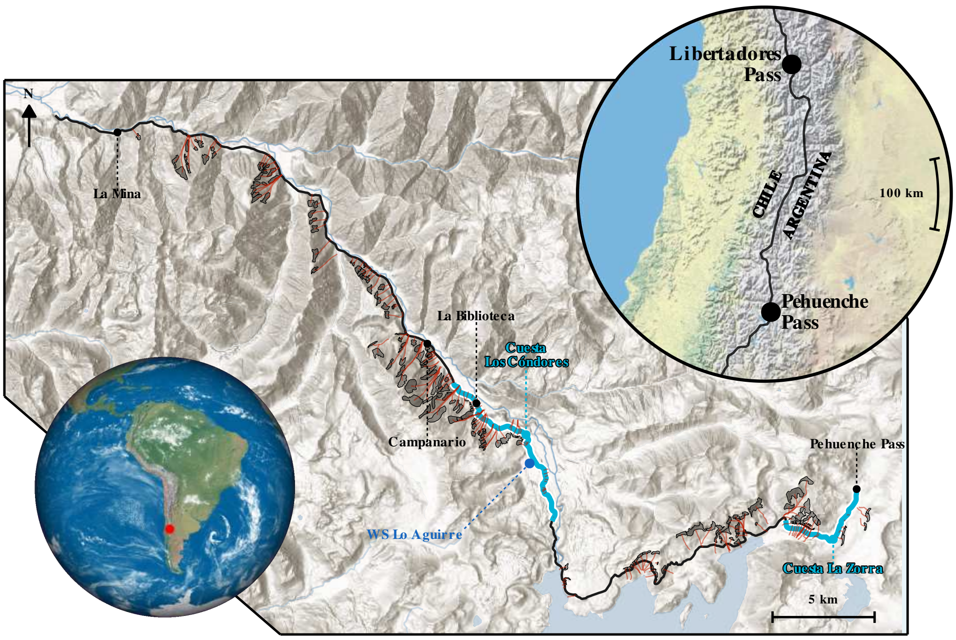

Figure 1. Study area: Route 115-CH from La Mina to Pehuenche Pass (61 km, Maule Region, Chile). The 208 avalanche release areas, simulated thalwegs (red), and the Lo Aguirre weather station (blue marker) are marked. Upper-right inset: regional setting with the Libertadores and Pehuenche border crossings; lower-left inset: location within South America. Basemap tiles: Esri World Hillshade (main map) and Esri World Physical (upper-right inset); sources: Esri, USGS, NGA, NASA, CGIAR, Intermap | Powered by Esri. Globe imagery: Natural Earth III (public domain).

https://doi.org/10.5194/egusphere-2026-3951
Preprint. Discussion started: 14 July 2026

3 Data and methods

3.1 Three snow-depth scenarios

The corridor-scale analysis is organized around three snow-depth scenarios, defined by the return period of the three-day new-snow-depth increase ($\Delta \mathrm{HS}_3$): *Moderate* ($T_{\mathrm{HS}} = 10\,\mathrm{yr}$), *Severe* ($T_{\mathrm{HS}} = 30\,\mathrm{yr}$), and *Extreme* ($T_{\mathrm{HS}} = 100\,\mathrm{yr}$). These return periods characterize snow-depth loading, not the probability of avalanche release: release depends on snowpack stability, temperature, wind loading and stratigraphy (Schweizer et al., 2008). The three return periods therefore bracket increasing intensities of snow loading rather than frequencies of avalanche occurrence; results are presented as peak-pressure and source-zone-count profiles, not as formal hazard-zone classifications.

Impact intensity at the road is classified following Bertrand et al. (2010): low ($<3\,\mathrm{kPa}$), medium (3–30 kPa), high (30–100 kPa), and very high ($>100\,\mathrm{kPa}$). Pressures above 30 kPa destroy light wood-frame structures (Keylock and Barbolini, 2001); we adopt this level as an indicative threshold for the onset of severe vehicle damage, and 100 kPa, above which most undefended structures fail (Keylock and Barbolini, 2001; Bertrand et al., 2010), as indicative of near-complete vehicle destruction.

3.2 Release area digitization and snow-depth estimation

The MOP avalanche study (Dirección de Vialidad, 2021) provided release area maps in PDF format only. We georeferenced 157 maps in QGIS using the Georeferencer tool. Initial polygon digitization was assisted by the Bunting Labs AI Vectorizer plugin for QGIS (Bunting Labs, 2024), which autocompletes polygon and line tracing on raster backgrounds. All AI-assisted polygons were reviewed and corrected manually. Release areas were originally delineated by Dirección de Vialidad (2021) combining expert geomorphological assessment, slope-angle criteria (critical range 30–50°), qualitative indicators (slope aspect, topographic breaks, NW wind-loading exposure), satellite-image analysis, and field observations from three winter seasons (2016–2018), together with operational records from *Dirección de Vialidad* personnel. This process produced a GIS database of 208 avalanche paths with associated release areas, fracture depths, and volumes for the three scenarios defined in Sect. 3.1; the digitized database is published as an open data set (Latorre, 2026).

Fracture depths for each scenario were derived by Dirección de Vialidad (2021) from a site-specific nivometeorological model. Reference snowfall values for the 2 000 m elevation band, calibrated against the Lo Aguirre station (DGA, 1953–2017), were assigned per return period using storm durations of 2, 2.5 and 3 days for $T = 10$, 30 and 100 yr respectively (110, 122 and 140 cm at 2 000 m). Values were then extrapolated by elevation (+6 % per 100 m above 2 000 m, with reductions below 1 600 m), corrected for slope angle (factor from 0.80 at 28° to 0.37 at 50°), and scaled by an expert-based wind-loading multiplier on northwest-facing leeward slopes. The release density ρ_0 was set to $250\,\mathrm{kg\,m^{-3}}$ for all three scenarios, based on the recently fallen snow density reported for the sector by Dirección de Vialidad (2021).

https://doi.org/10.5194/egusphere-2026-3951
Preprint. Discussion started: 14 July 2026

3.3 Event reconstruction

While additional avalanche events have been documented along Route 115-CH, only four cases on two paths provide the combination of release-zone delineation, fracture depth, deposit measurements, and runout extent required for back-analysis calibration. Chile lacks a systematic avalanche register comparable to those maintained in Switzerland or Austria, and observational records elsewhere on the corridor are limited to anecdotal photographs and post-event interventions. The Campanario 2011 event is particularly valuable because video documentation, deposit-height measurements, and a delineated deposition area constrain the large-volume regime that dominates exposure on this corridor. The four selected events are summarized below, with each path providing a calibration/validation pair (Table 1, Fig. 2):

1. **Campanario** (path A36-1, Quebrada Campanario, km 125).

   Calibration event (2 October 2011). A wet full-depth slab avalanche reached the road with 3–4 m deposit heights, bending the containment barrier (Dirección de Vialidad, 2021). The deposition area is identified here for the first time using the Normalized Difference Snow Index (NDSI > 0.5; Hall and Riggs, 2011) computed from Landsat 5 imagery (9 October 2011). This is the largest documented event on the route. The release density ρ_0 was set to 470 kg m^{-3}, based on the historical October mean from the DGA Lo Aguirre nivometric site located within the same valley system. This monthly mean was used as a proxy in the absence of a measurement on the event date.

   Validation event (2 July 2022). A powder-snow avalanche released on the same path following two successive storm fronts (Viento Puelche, 2022), with 1.8 m deposit heights, a runout of $\sim$1.7 km, and an estimated release volume of $\sim$9 100 m^3 (size class 3). A snow pit excavated the same day at nearby Cerro La Biblioteca revealed a 152 cm snowpack with a surface-hoar weak layer; a compression test (CT12) produced an abrupt planar fracture at 78 cm depth, constraining the slab thickness to $\sim$78 cm of recent low-cohesion snow with a release density of $\sim$200 kg m^{-3}. Both calibration and validation events on the Campanario path are simulated as dense-flow avalanches with com1DFA, since the module is not designed to represent the powder component. For the 2022 event, the dense core morphology and runout are used for comparison, whereas the powder cloud (visible in video records) is acknowledged separately as a non-modeled feature (Sect. 4.1).

2. **La Biblioteca** (path A44, km 130).

   Calibration event (7 October 2018). A 50 cm slab released $\sim$3 200 m^3 and deposited 2–3 m of snow on the road. The release density ρ_0 was set to 250 kg m^{-3}, based on the recently fallen snow density reported for the sector by Dirección de Vialidad (2021). Temperature records from the Pique de Válvulas nivological station (Viento Puelche, 2018; $\sim$200 m above La Biblioteca) show a marked temperature increase preceding the event, suggesting that warming was a contributing trigger.

   Validation event (15 October 2018). An adjacent slab (70 cm thick, $\sim$2 800 m^3) produced 3–5 m deposits and reached the river bank, as observed in post-event photographs (Dirección de Vialidad, 2021). Both events followed temperature increases recorded at Pique de Válvulas.

https://doi.org/10.5194/egusphere-2026-3951
Preprint. Discussion started: 14 July 2026

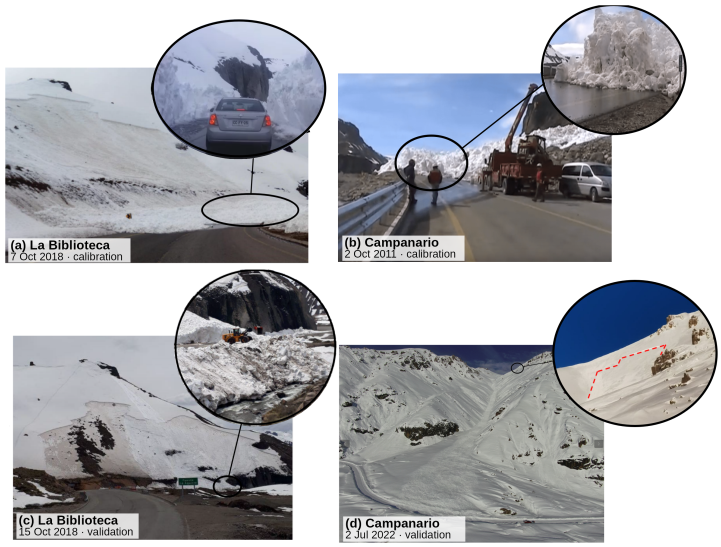

Figure 2. Field photographs of the four back-analysis events (cf. Table 1). Circular insets zoom on deposit details and the road impact; in the Campanario 2 Jul 2022 panel (bottom right), the dashed red line outlines the digitized release area. Photo credits: Dirección de Vialidad (2021), Viento Puelche (2022).

Table 1. Observed and back-analysis data for the four documented events on two paths. C = calibration, V = validation. Elevation range, horizontal path length, and mean slope are measured on the model DEM from the release crown to the road (Campanario: along the digitized thalweg; La Biblioteca: along the fall line).

Path	Date	Role	Elev. range (m)	Length (m)	Slope (°)	Depth on road (m)	Runout observation	Release source	Fracture (cm)	Volume (m^3)
Campanario	2 Oct 2011	C	2446–1569	2010	24	3–4	Barrier impact	Simulated (back-an.)	60 (back-an.)	∼65 000 (back-an.)
Campanario	2 Jul 2022	V	2379–1569	1930	23	1.8	Road + barriers	Photos	∼78	∼9 100
La Biblioteca	7 Oct 2018	C	2009–1941	100	34	2–3	Road deposit	Photos	50	∼3 200
La Biblioteca	15 Oct 2018	V	1994–1936	88	34	3–5	River bank	Photos	70	∼2 800

https://doi.org/10.5194/egusphere-2026-3951
Preprint. Discussion started: 14 July 2026

3.4 Numerical model: AvaFrame com1DFA

We performed all numerical simulations using the dense-flow module com1DFA of AvaFrame (v1.8, commit 5962b0d0) (Tonnel et al., 2023; Oesterle et al., 2024), a thickness-integrated computational avalanche model whose basal friction builds on the Voellmy framework (Voellmy, 1955). We used the `samosATAuto` friction parameterization (Sampl, 2007; Sampl and Granig, 2009), which automatically selects one of three parameter sets (standard, small, or medium) based on the release volume. The shear stress $\tau^{(b)}$ is expressed as:

$$\tau^{(b)} = \tau_0 + \tan\delta \left(1 + \frac{R_s^0}{R_s^0 + R_s}\right)\sigma^{(b)} + \frac{\rho_0\,\bar{u}^2}{\left(\frac{1}{\kappa}\ln\frac{\bar{h}}{R} + B\right)^2} \quad (1)$$

where $\tan\delta = \mu$ is the Coulomb friction coefficient, $\sigma^{(b)}$ is the normal stress at the base, ρ_0 is the mean column density, $\bar{u}$ the depth-averaged velocity, and $\bar{h}$ the flow depth. The parameters τ_0 (minimum shear stress), $R_s^0 = 0.222$, $R = 0.05$, $B = 4.13$, and $\kappa = 0.43$ are empirical constants from Sampl (2007), $\tau_0 = 0$ in the standard calibration, so creep suppression is governed entirely by the fluidization ratio $R_s = \rho_0\bar{u}^2/\sigma^{(b)}$. Preliminary tests with the standard Voellmy formulation showed that this creep led to excessive lateral spreading; the `samosATAuto` parameterization was therefore preferred. Although this thickness-integrated approach simplifies the vertical velocity profile, chute experiments and field measurements at instrumented sites such as Vallée de la Sionne show that the actual profile varies with position along the flow (Schaefer et al., 2010; Sovilla et al., 2008).

The com1DFA module was originally calibrated against documented large-volume avalanches in the European Alps (primarily Austrian sites for SAMOS-AT, Swiss sites for RAMMS), in the range $V > 30\,000\,\mathrm{m}^3$ (Sampl, 2007; Sampl and Granig, 2009; Tonnel et al., 2023). Several paths on Route 115-CH (notably La Biblioteca, $V \approx 2\,800$–$3\,200\,\mathrm{m}^3$) fall well below this range, requiring path-specific friction calibration as described in Sect. 3.5 and discussed further in Sect. 5.3.

For each simulation, com1DFA produces raster outputs of peak flow thickness (pft, m), peak flow velocity (pfv, $\mathrm{m\,s^{-1}}$), and peak pressure (ppr, Pa). Pressure is computed as $p_{\mathrm{peak}} = \rho_0\,\bar{u}^2$ from the thickness-averaged variables. com1DFA assumes a constant flow density equal to the prescribed release density ρ_0, so the same value enters the friction relation (Eq. 1) and the pressure diagnostic. Throughout this study, we use ppr as the primary intensity metric at road-crossing locations, pft for deposit-height comparisons during back-analysis, and pfv when assessing dynamic effects. Time-step rasters of flow thickness at 1 s intervals are also generated and used for arrival-time analyses (Sect. 3.7). Recent work shows that run-up height and the vertical pressure distribution on narrow obstacles are governed by distinct mechanisms not captured by thickness- or depth-averaged ppr (Kohler et al., 2026), as discussed in Sect. 5.3.

Table 2 summarizes all com1DFA input parameters and DEM sources used in this study.

3.5 Calibration strategy

The present calibration varies only the Coulomb friction μ, as Fischer et al. (2015) showed that μ exhibits the strongest correlation with runout distance among all friction parameters. A multivariate optimization should be pursued once additional calibration events become available (Sect. 5.3).

https://doi.org/10.5194/egusphere-2026-3951
Preprint. Discussion started: 14 July 2026

Table 2. Summary of com1DFA simulation parameters and input data.

Parameter	Campanario		La Biblioteca		Route 115-CH
	Calibration (2 Oct 2011)	Validation (2 Jul 2022)	Calibration (7 Oct 2018)	Validation (15 Oct 2018)	Extrapolation (208 paths)
DEM	12.5 m (ALOS PALSAR)		1 m (survey contours, MOP 2021)		12.5 m (ALOS PALSAR)
Friction μ	0.20 (modeled best fit)	0.20 (modeled best fit)	0.31 (modeled best fit)	0.31 (modeled best fit)	0.20 / 0.31 (sensitivity ±15 %)
Modeled density ρ_0 (kg m^{-3})	470[a]	200[b]	250[c]	250[c]	250[d] (sensitivity ±150)

[a] Historical October mean snow density at the DGA Lo Aguirre nivometric station. [b] Estimated from snow pit (Viento Puelche, 2022). [c] Estimated for the sector by Dirección de Vialidad (2021). [d] Regional value (Dirección de Vialidad, 2021).

The calibration strategy is designed around two paths, each with a calibration event and an independent validation event (Table 1). Given the limited boundary conditions for each event, we varied μ to match observed deposit heights and runout extent. For Campanario, we ran 130 simulations with $\mu \in [0.10, 0.30]$ and fracture depths between 0.1 and 1.0 m (release volumes ~11 000–108 000 m^3). Valid simulations were required to satisfy: (i) deposit heights of 3–4 m at the road centerline; (ii) the deposit mass center within the deposition area derived from satellite images; and (iii) no underestimation of the deposition extent. The third criterion favors runout overestimation over underestimation, providing a conservative bias for road exposure assessment.

For La Biblioteca, the smaller release volume motivated a search range shifted toward higher friction values, $\mu \in [0.20, 0.40]$, consistent with the volume–friction trend reported by Naaim et al. (2013) and Fischer et al. (2015) in which smaller avalanches exhibit higher effective friction. The 7 October event served for calibration (2–3 m deposits on road), and the 15 October event for independent validation (3–5 m deposits, runout to river bank).

3.6 Corridor-scale simulation and automated thalweg extraction

Having calibrated friction from the two reference paths, we extended the analysis to the full 208 paths of the corridor. The calibrated μ values were extrapolated based on release volume under the *Severe* scenario: paths with release volumes $\leq 10\,000$ m^3 were assigned $\mu = 0.31$ (La Biblioteca calibration), while larger paths received $\mu = 0.20$ (Campanario calibration). The split was implemented through the volume classification of the `samosATAuto` friction model, with the class boundary set to 10 000 m^3 and the class-specific μ values replaced by the calibrated ones. Only the Coulomb friction coefficient μ was therefore overridden from the back-analysis calibration; all other SAMOS-AT parameters (τ_0, R_s^0, κ, B, R) were kept at their com1DFA default values, identical across volume classes (Tonnel et al., 2023; Oesterle et al., 2024). Each of the 208 paths was simulated under the three scenarios defined in Sect. 3.1 (*Moderate*, *Severe*, *Extreme*), yielding 624 simulations in total.

https://doi.org/10.5194/egusphere-2026-3951
Preprint. Discussion started: 14 July 2026

AvaFrame com1DFA includes native batch processing via the `runCom1DFA` workflow (Tonnel et al., 2023; Oesterle et al., 2024). To scale efficiently to 208 paths and 624 simulations on a high-performance cluster, we developed a Python wrapper that partitions the corridor into 24 independent computational zones, each containing 5–12 paths, allowing parallel execution and per-zone configuration overrides.

Avalanche thalweg lines were extracted automatically from the simulation results using a hybrid two-stage algorithm developed in this work. The native com1DFA thalweg extractor tracks the flow mass center, which underestimates the runout because the deposit front advances beyond the center of mass. We therefore extended the mass-center trajectory to the deposit front via a Dijkstra least-cost path (Dijkstra, 1959) targeting the flow-thickness-weighted centroid of the lowest 5 % elevation band within the flow footprint (peak flow thickness > 0.01 m). We validated the algorithm against 208 manually delineated reference thalwegs for the *Severe* scenario. The median absolute distance between automated and manual endpoint locations is 64 m. Of the 208 paths, 80.3 % (167 paths) match the reference within 100 m, and 91.3 % (190 paths) within 150 m.

To assess the sensitivity of the corridor-scale results to friction and density assumptions, two additional simulation sets were run. First, the Coulomb friction coefficient μ was perturbed by ± 15 % ($\mu_{\text{low}} = 0.17/0.26$; $\mu_{\text{high}} = 0.23/0.36$ for large/small paths, respectively), yielding 1 248 additional simulations (624 per perturbation). This range agrees with back-calculation scatter reported across European test sites (Barbolini et al., 2000; Barbolini and Savi, 2001), the Monte Carlo posterior distributions of Ancey (2005), and the snow-property-dependent variability documented by Naaim et al. (2013); Salm et al. (1990) noted that μ in the Voellmy model can vary by $\sim$20 % depending on snow temperature and moisture content. Second, the release density ρ_0 was perturbed by $\pm 150\,\mathrm{kg\,m^{-3}}$ from the baseline $\rho_0 = 250\,\mathrm{kg\,m^{-3}}$, yielding $\rho_0 = 100\,\mathrm{kg\,m^{-3}}$ (low bound) and $\rho_0 = 400\,\mathrm{kg\,m^{-3}}$ (high bound), adding 1 248 simulations (624 per density). In total, 3 120 simulations (baseline plus four sensitivity configurations) were run.

3.7 Road exposure analysis

For each of the 624 baseline simulations, we extracted the road-crossing peak pressure: the maximum value of the simulated peak pressure raster (hereafter ppr) within a 50 m buffer of the road centerline, sampled at 10 m intervals along the road. Events with maximum ppr $>$10 Pa at any sample point were classified as road-reaching simulations. We adopt this low threshold ($\sim$ instrument noise level) to capture the geometric reach of any avalanche deposit at the road; a higher threshold (e.g. the AIMEC default of 1000 Pa) would exclude only marginal cases without materially affecting the corridor-scale results. A single road sample point exceeding the threshold suffices for classification.

Road exposure was quantified at the path level (binary: road reached or not) and at the route level using a 1 km chainage grid. We distinguish two terms: a *catchment* (source zone) is an independent topographic release basin, whereas a *sub-path* is one of the 208 simulated release areas, several of which may discretize a single wide catchment. For each 1 km segment k, the number of avalanche sub-paths N_k is the count of the 208 sub-paths that produce ppr $>$10 Pa on that segment under at least one of the three scenarios (Sect. 3.1); where relevant we also report the number of distinct parent catchments. The *scenario crossing count* $n_k^{(s)}$ records the number of simulations reaching segment k under scenario s specifically. These metrics characterize

https://doi.org/10.5194/egusphere-2026-3951
Preprint. Discussion started: 14 July 2026

where avalanche paths converge on each road segment and the minimum scenario (snow-loading level) at which a path first reaches the road, without implying any specific avalanche occurrence frequency.

Road-crossing intensities follow the classes defined in Sect. 3.1 (Bertrand et al., 2010). We used these classes to estimate the proportion of events capable of damaging or destroying a vehicle, supporting risk prioritization.

Arrival times were extracted from the same simulation outputs by analyzing the flow-thickness time-step rasters (1 s intervals) for all 624 simulations, using the same road-reaching criterion (ppr >10 Pa at any road sample point). For each road-reaching simulation, the arrival time is defined as the first time step at which flow thickness exceeds zero at any of those road points.

4 Results

4.1 Campanario back-analysis

Of the 130 Campanario back-analysis simulations, 12 met all validation criteria. These correspond to a valid μ range of 0.18–0.22 (reference value 0.20) and release volumes of $\sim$54 000–86 000 m^3 (Fig. 3a, b). The reference model ($\mu = 0.20$, $V \approx$ 64 600 m^3) reproduces the NDSI-derived deposition area and the observed 3–4 m deposit heights on the road. Peak pressure at the road is $\sim$40 kPa, and the simulated arrival time at the road is approximately 2 min after release initialization. Automated Indicator-based Model Evaluation and Comparison (AIMEC) thalweg analysis (Fischer, 2013) indicates that the pressure variability across the calibration ensemble decreased along the path: $\pm$100 kPa in the upper track versus $\pm$20 kPa at road level, indicating that road-crossing peak-pressure estimates are robust to the spread of calibrated μ values, whereas upper-track values remain sensitive to the friction calibration.

An independent validation is provided by the 2 July 2022 event on the same path (see Sect. 3.3 for snowpack observations). The digitized release area ($\sim$11 700 m^2) yields an estimated volume of $\sim$9 100 m^3. Although roughly seven times smaller than the calibration event ($\sim$65 000 m^3) and close to the 10 000 m^3 class boundary used for the corridor extrapolation (Sect. 3.6), the event provides a temporally independent, same-path check of the friction value (see Sect. 5.3 for discussion of size-class transferability). Sixteen simulations with μ varied from 0.15 to 0.30 showed that models with $\mu = 0.18$–0.22 best reproduced the observed deposit, which reaches the road with heights of $\sim$1.8 m before the road barrier. Video recordings of the event confirm a mixed (dense core plus powder cloud) avalanche; the powder component projected several meters beyond the road, but this component is not captured by com1DFA. The dense deposit morphology and runout distance are nevertheless well reproduced (Fig. 3c), confirming $\mu \approx 0.20$ as representative for large avalanches on the Campanario path and completing the calibration–validation pair for this path.

4.2 La Biblioteca back-analysis

For the 7 October 2018 event ($V \approx 3\,200$ m^3; 18 simulations), the observed 2–3 m deposits on the road are reproduced over a broad friction range ($\mu \geq 0.28$; Fig. 3d, e); the reference model ($\mu = 0.31$) gives 2.8 m deposits, simulated pressures on the

https://doi.org/10.5194/egusphere-2026-3951
Preprint. Discussion started: 14 July 2026

carriageway of up to ∼50 kPa (≈20 kPa on average across the affected segment, as the flow runs oblique to the road) and arrival times <10 s due to the path's proximity to the road. The 15 October event ($V \approx 2\,800\,\mathrm{m}^3$), released from an adjacent area, provides the tighter constraint (Fig. 3f): $\mu = 0.30$–0.33 reproduces both the 3–5 m deposits and the runout to the river bank, with the reference model giving 3.8 m deposits and a peak pressure at the road of ∼43 kPa. Together, the two events constrain μ to 0.30–0.33 for small avalanches on this path.

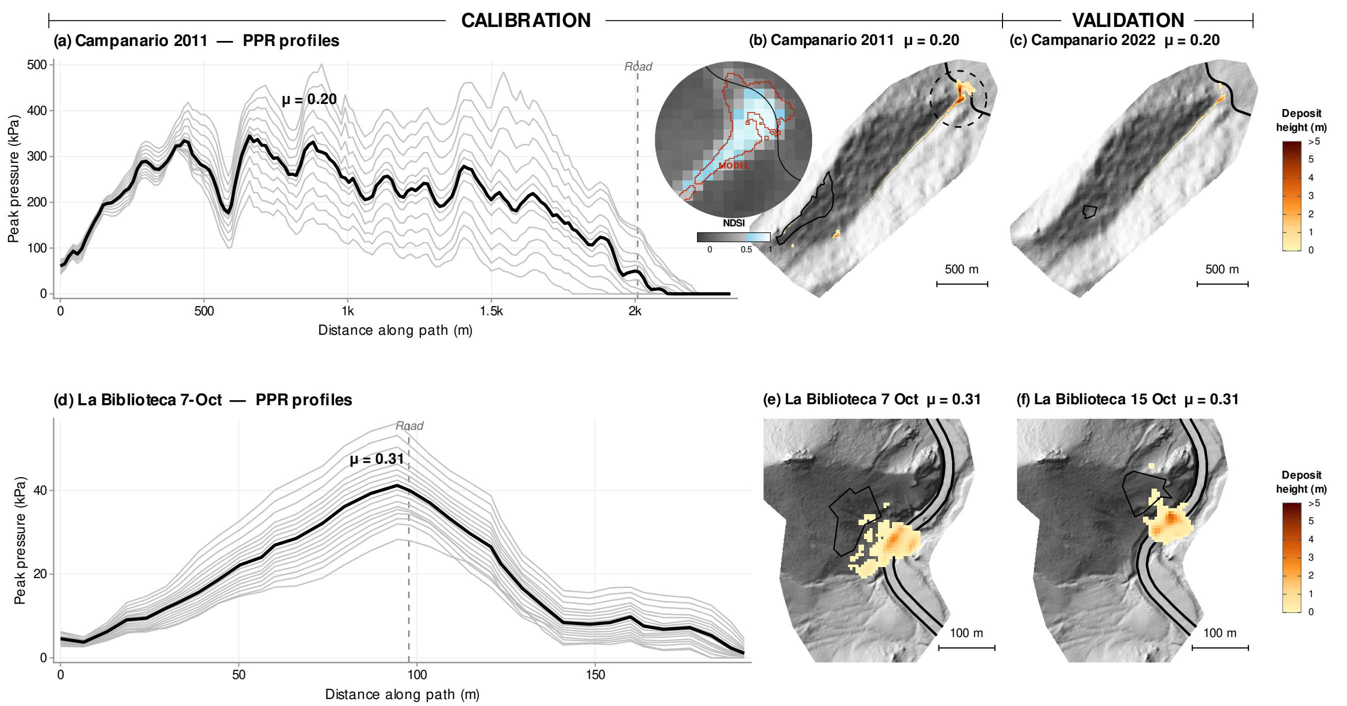

Figure 3. Back-analysis for the two calibration paths. Top row, Campanario: (a) peak-pressure profile (calibration ensemble $\mu \in [0.10, 0.30]$, gray; reference $\mu = 0.20$, black); (b) 2011 calibration deposit, inset showing the NDSI-derived snow extent against the simulated outline (red); (c) 2022 validation deposit. Bottom row, La Biblioteca: (d) profile (ensemble $\mu \in [0.20, 0.40]$, gray; reference $\mu = 0.31$, black); (e) 7 Oct 2018 calibration, (f) 15 Oct 2018 validation.

4.3 Corridor-scale intensity map

Figure 4 presents the avalanche intensity map for the entire Route 115-CH. From La Mina to Laguna del Maule, the road is located predominantly in deposition zones, while from Laguna del Maule to Pehuenche Pass it traverses mainly transit zones where higher velocities and pressures are expected. Most of the exposed sections experience ppr >30 kPa under the *Moderate* or *Severe* scenarios. The section immediately upstream of La Mina and isolated valley-floor segments near the border show lower intensities or no simulated impact due to topographic shielding or reduced runout at small volumes.

https://doi.org/10.5194/egusphere-2026-3951
Preprint. Discussion started: 14 July 2026

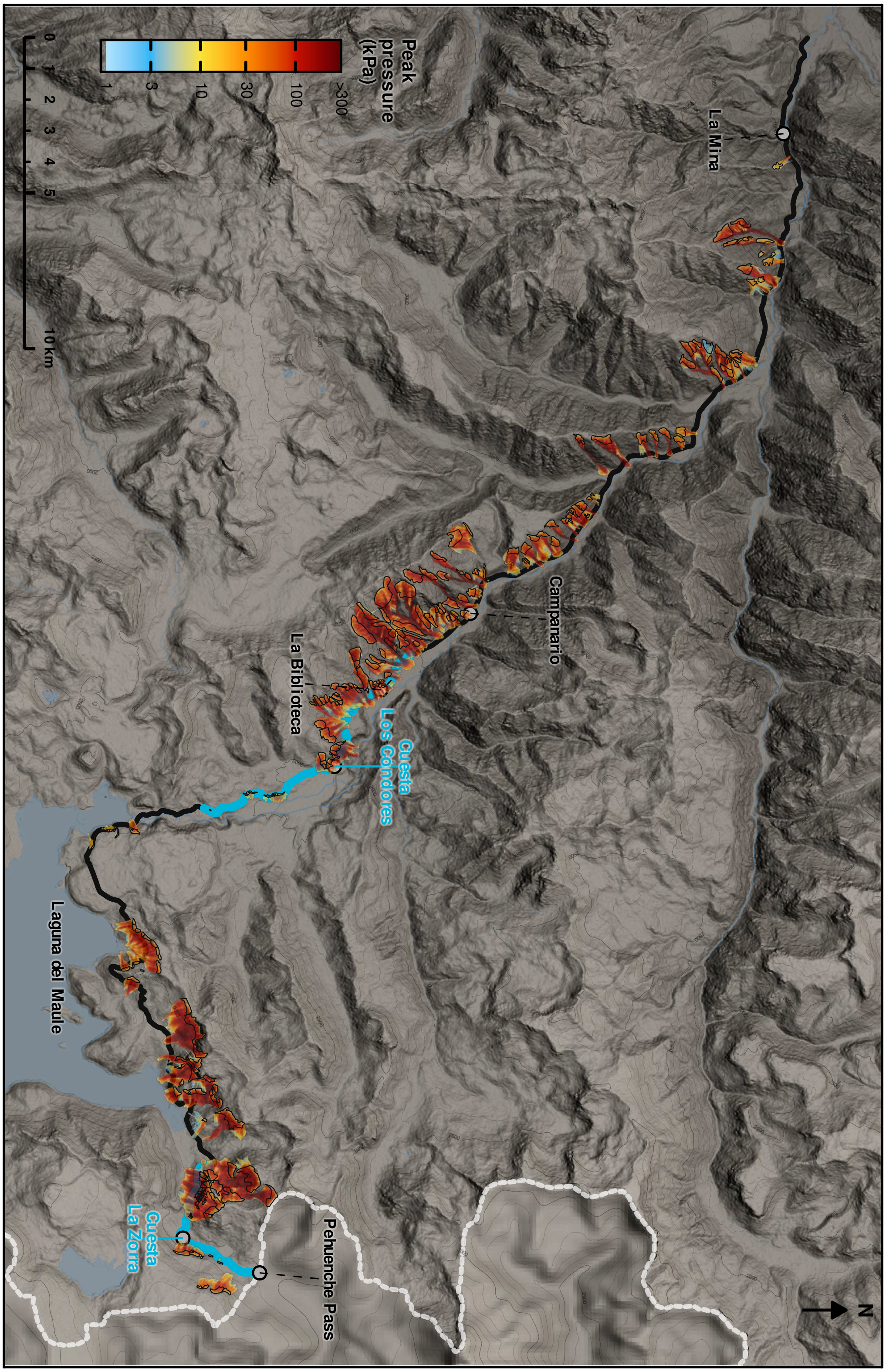

Figure 4. Avalanche intensity map for Route 115-CH (*Severe* scenario, $T_{\mathrm{HS}} = 30$ yr): maximum peak pressure envelope across all 208 simulated paths (color scale saturated at 300 kPa). Release areas are outlined in black.

https://doi.org/10.5194/egusphere-2026-3951
Preprint. Discussion started: 14 July 2026

4.4 Quantitative road exposure profile

Hot-spots are quantified by the number of simulated avalanche sub-paths reaching each road segment, matching the per-km counts in Fig. 5b; for each we also give the number of distinct parent catchments, since a single wide catchment may be discretized into several sub-paths (e.g. catchment A68 places 14 of its 17 sub-paths on the km 155 segment, and A9–A11 the 11 sub-paths at km 110). All km values reported below refer to the official kilometrage of Route 115-CH (Retén La Mina at km 101, Pehuenche Pass at km 161.5); the modeled 61 km section spans approximately km 98–159, beginning ∼3 km below the Retén and ending ∼3 km before the Pass.

Of the 624 corridor-scale simulations (one thalweg per simulation), 527 (84 %) reach the road (maximum ppr >10 Pa at any road sample point). Expressed as road length physically reached, exposure grows with scenario severity: 19.6 km (32 % of the 61 km corridor) under the *Moderate* scenario, 21.8 km (36 %) under *Severe*, and 24.7 km (40 %) under *Extreme* (Fig. 5b). Even under *Extreme*, about 36 km (60 %) of the corridor remain topographically shielded or beyond the runout limit of all modeled paths.

The number of sub-paths reaching each km segment ranges from zero in the shielded sections to $N_{k,\max} = 14$ at km 155, where 14 sub-paths of a single wide catchment (A68, discretized into 17 sub-paths, all of which reach the road) cross within the same kilometer (Fig. 5b). The spatial pattern is markedly non-uniform: hazard is concentrated in distinct clusters separated by shielded gaps, reflecting the transverse valley topography. Six segments stand out as primary hot-spots (sub-paths; distinct parent catchments in parentheses): km 155 (14 sub-paths, 1 catchment), km 110 (11; 3 catchments, A9–A11), km 127–128 (10 and 8; A38–A41, within Cuesta Los Cóndores), km 105 (8; 4 catchments), km 122 (8; 3 catchments, A28–A30), and km 125 (8; at Campanario).

4.4.1 Peak pressure intensity at road crossings

Peak pressure at road-crossing points reaches up to 477 kPa, with a median of 75 kPa across all 527 road-reaching simulations (Table 3). The median peak pressure increases from 61 kPa (*Moderate*) to 104 kPa (*Extreme*), reflecting the increase in release volume with scenario severity. Applying the intensity thresholds of Sect. 3.7: 77 % of all road-crossing events exceed the 30 kPa vehicle-damage threshold, and 41 % exceed the 100 kPa vehicle-destruction threshold (Table 3).

Spatially, the highest peak pressure values occur in the upper corridor (km 138–159), where transit-zone crossings are more common, and in the km 120–130 cluster. In the lowermost corridor (km 98–117), crossings tend to occur in deposition zones, resulting in lower velocities and pressures but higher deposit depths, implying a different damage mechanism (burial and road obstruction rather than dynamic impact). The most exposed segments combine the highest source-zone convergence with the highest median peak pressures.

4.5 Arrival times at road crossings

Of the 624 baseline simulations, 527 reach the road. The median simulated arrival time is 25 s, with a mean of 33 s and a range of 0–145 s (Fig. 5e). More than half (51 %) of road-reaching paths arrive within 30 s of release, 83 % within 60 s, and

https://doi.org/10.5194/egusphere-2026-3951
Preprint. Discussion started: 14 July 2026

Table 3. Peak pressure (ppr) at the road for the 527 road-reaching simulations on Route 115-CH, by scenario. Intensity classes follow Bertrand et al. (2010).

		ppr at road (kPa)			ppr ≥ 30 kPa
Scenario	n	Median	P75	Max	%
Moderate	162	61	111	348	69 %
Severe	176	71	142	412	76 %
Extreme	189	104	197	477	85 %

virtually all (99 %) within 120 s. Arrival times decrease with scenario severity: median 30 s (*Moderate*), 27.5 s (*Severe*), and 25 s (*Extreme*), reflecting the higher velocities associated with larger release volumes. The shortest arrival times (<30 s) are concentrated in the upper corridor (km 138–159), where steep, short paths discharge directly onto the road.

4.6 Corridor-scale exposure synthesis

Figure 5 synthesizes the corridor-scale exposure analysis along the full 61 km of Route 115-CH. The schematic plan view (panel a) locates key landmarks along the corridor. Road-reaching paths per kilometer are stacked by triggering scenario in panel (b), where each of the 189 paths is counted once at its lowest reaching scenario (162 Moderate, 15 Severe-only, 12 Extreme-only); this incremental count differs from the per-scenario road-reaching counts in Table 3. Panels (c) and (d) show simulated runout length and peak pressure, respectively; in panel (d), red dots mark *Severe*-scenario crossings exceeding the 30 kPa vehicle-damage threshold. Panel (e) presents arrival times, with red dots for *Severe*-scenario arrivals within 60 s of release.

The highest path convergence, peak pressures and shortest arrival times are concentrated between km 105 and km 130 (around Campanario and La Biblioteca) and at km 155 in Cuesta La Zorra (where 14 sub-paths of a single catchment, A68, reach the road). The upper corridor (km 138–159) overall combines short steep paths with high peak pressures and sub-minute arrival times (panels b–e).

https://doi.org/10.5194/egusphere-2026-3951
Preprint. Discussion started: 14 July 2026

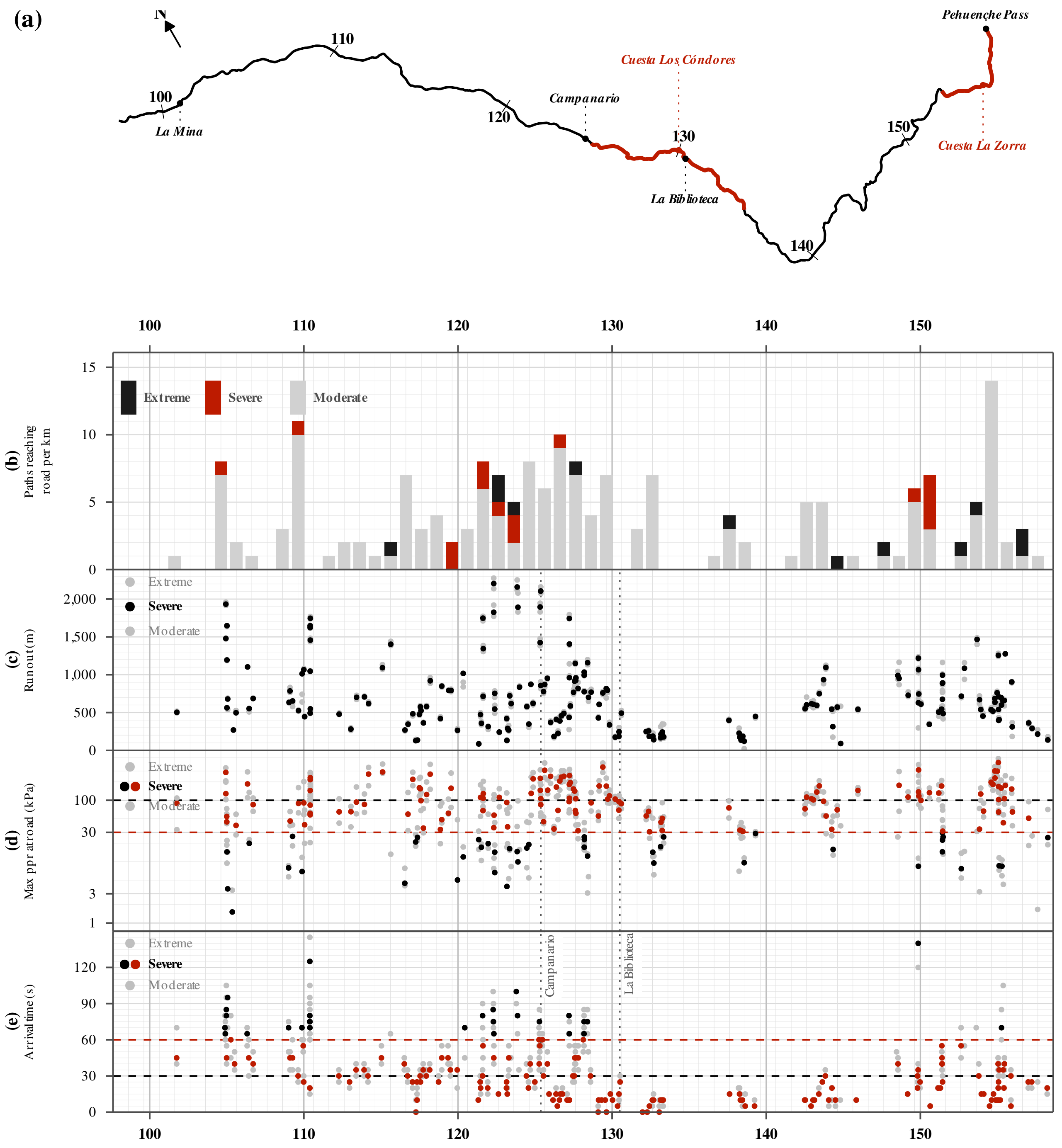

Figure 5. Corridor-scale exposure synthesis for Route 115-CH. (a) Schematic plan view. (b) Paths reaching the road per km, stacked by the minimum scenario at which each path first reaches it (each path counted once). (c) Runout length, (d) peak pressure (log scale), (e) arrival time per crossing. Dotted vertical lines across (c)–(e), labeled at the (d)/(e) boundary, mark the road crossings of the two calibration paths (Campanario and La Biblioteca). In (d) and (e), red marks *Severe*-scenario crossings ≥ 30 kPa and arrivals ≤ 60 s; dashed lines mark the 30/100 kPa and 30/60 s reference thresholds.

https://doi.org/10.5194/egusphere-2026-3951
Preprint. Discussion started: 14 July 2026

5 Discussion

5.1 Friction calibration in the context of Chilean avalanche studies

The calibrated values ($\mu = 0.18$–0.22 for Campanario and $\mu = 0.30$–0.33 for La Biblioteca) follow the general pattern of lower friction for larger avalanches (Ancey, 2005) and are compatible with previous studies in the Chilean Andes. However, direct comparison of Coulomb friction values across studies must be made with caution, because the different models used in the Chilean Andes (SAMOS-AT in this work, Voellmy μ–ξ in RAMMS, temperature-dependent friction in RAMMS + SNOWPACK) employ different friction formulations and parameters are not directly transferable between them (Martini et al., 2023). With this caveat, the few published Chilean studies show a coherent pattern. Janeras et al. (2013) back-analyzed large historical avalanches at Sewell (central Chilean Andes) with Aval-1D and RAMMS, obtaining Voellmy $\mu \approx 0.18$–0.25 for the dense flow. Vera Valero et al. (2016, 2018) modeled wet-snow runout at a high-altitude Andean mine site with RAMMS coupled to SNOWPACK and showed that temperature-dependent friction substantially improves runout prediction, with effective $\mu \approx 0.29$–0.50 for the smaller wet-snow events. The Route 115-CH calibration falls within this same pattern (lower μ for larger volumes) and is consistent with European volume–friction relationships (Fischer et al., 2015; Barbolini et al., 2000; Naaim et al., 2013).

A direct, kilometer-aligned comparison with the *Dirección de Vialidad* assessment (Dirección de Vialidad, 2021) is instructive. At equal return period (30 years) and release density (250 $\mathrm{kg\,m^{-3}}$), our model reproduces its peak pressures within 5–10 % wherever it assumed a medium size class (A20, A39, A68; e.g. A68/Cuesta La Zorra, 392 vs. 412 kPa), but exceeds them 3.5–6.0 times where it assumed a small class (A37, A38, A42 in Cuesta Los Cóndores; e.g. A42, 100 vs. 347 kPa). The *Dirección de Vialidad* modeled pressures for only seven of the 65 release zones that its own study identified as reaching the road. Despite recording a large wet-snow avalanche at Campanario in 2011 (our calibration event, ≈65 000 $\mathrm{m^3}$, "very large" on its own scale), it assigned that sector a medium design magnitude with no dynamic modeling. Because these pressures feed the structural loads of the planned galleries, four compounding factors bias them low: the Alpine-derived RAMMS default friction ($\mu \approx 0.23$–0.25 against our calibrated 0.20 for large channeled paths), a density fixed at 250 $\mathrm{kg\,m^{-3}}$, release depths inferred from only three winters, and a lone calibration check (the La Biblioteca events) whose release area we reconstruct at about half the adopted value. The design basis at the small-classed and unmodeled zones is therefore systematically below what a corridor-scale deterministic model yields.

The volume-dependent extrapolation using two anchor points is a deliberate simplification. The actual μ–V relationship is continuous and path-specific (Fischer et al., 2015); the discrete split at 10 000 $\mathrm{m^3}$ provides internal consistency across scenarios. Within the large-volume regime, Campanario 2011 ($V \approx 65\,000\,\mathrm{m^3}$) anchors the calibration; no events with $V > 100\,000\,\mathrm{m^3}$ were available, leaving the largest-volume paths (up to $V \approx 770\,000\,\mathrm{m^3}$ in the *Extreme* scenario) constrained only by extrapolation. This is the primary source of systematic uncertainty in the corridor simulations.

Gauer et al. (2010) showed, from a dataset of ∼300 extreme avalanches across Norway, Austria, and Canada, that volume variation of two orders of magnitude produces less than 50 % runout variation, suggesting that friction mechanisms, rather than mass, are the primary control on runout. This lends qualitative support to our use of a single $\mu = 0.20$ across large-volume paths, although it does not by itself validate the specific 10 000 $\mathrm{m^3}$ class boundary.

https://doi.org/10.5194/egusphere-2026-3951
Preprint. Discussion started: 14 July 2026

5.2 Road exposure: extent, spatial pattern, and intensity

5.2.1 Extent and comparison with international studies

About two-fifths of Route 115-CH (24.7 of 61 km in the *Extreme* scenario) lies within reach of at least one simulated avalanche. Direct comparison with other corridors is complicated by differing exposure metrics. The most methodologically similar study, Wastl et al. (2011), modeled statistical runout on a 38.7 km Icelandic road and found roughly 9 km (∼23 %) within avalanche reach under their worst-case scenario. Regional historical-inventory assessments (Leone et al., 2014, across the French Alps) and site-count studies (Hao et al., 2023, 64 avalanche-prone sites along 20 km of the G218 highway) quantify exposure differently and are not directly comparable in length terms. The exposure of Route 115-CH is concentrated by the narrow valley geometry, where the road occupies most of the valley floor and steep high-elevation catchments rise directly above the carriageway.

Because path counts cluster strongly along the route, mitigation resources can be concentrated where they matter most. The top six hot-spot segments together represent only about 7 km (11 %) of the route but concentrate the greatest number of sub-paths reaching the road: km 155 (14 sub-paths from a single catchment, A68, Cuesta La Zorra sector); km 110 (11 sub-paths from three catchments, A9–A11); km 127–128 within Cuesta Los Cóndores (A38–A41); km 122 and km 125 just below and at Campanario; and km 105 in the lower corridor. Conversely, about 36 km of route remain shielded under every scenario, providing natural reference sections where closures would be unnecessary from an avalanche perspective.

5.2.2 Warning time and near-road releases

Warning time is near zero for release areas close to the road. The La Biblioteca path illustrates this extreme: with a release area approximately 100 m upslope of the road, the avalanche reaches the carriageway in less than 10 s. Conventional remote sensing or observer-based warning systems cannot provide adequate lead time for evacuation in such configurations.

With 83 % of road crossings arriving within 60 s of release (Sect. 4.5), most avalanche–road interactions leave effectively no time for warning-based evacuation. For these crossings, effective risk reduction requires either preventive road closure during and shortly after snowfall events, or structural protection (galleries, deflectors) rather than warning-based approaches (Glaus et al., 2025). Only the remaining 17 % of crossings, with arrival times exceeding 60 s, could potentially be managed through detection-triggered gate closures. This warning-time dimension is absent from the existing *Dirección de Vialidad* assessment, which reported only static pressures and runout; the corridor-wide arrival-time analysis presented here is, to our knowledge, the first for Route 115-CH, and it is what determines, segment by segment, whether preventive closure or permanent structural protection is the appropriate response.

5.2.3 Impact intensity and vehicle damage

About 77 % of all simulated road-crossing events exceed the 30 kPa vehicle-damage threshold. At 30 kPa, Keylock and Barbolini (2001) report that structural damage to standard vehicles begins; at 100 kPa (exceeded in 41 % of events) near-complete

https://doi.org/10.5194/egusphere-2026-3951
Preprint. Discussion started: 14 July 2026

vehicle destruction can be expected. These proportions imply that most avalanche arrivals at Route 115-CH carry sufficient energy to damage or destroy a vehicle present at the time of impact. The increase in both median peak pressure and the proportion of events exceeding the 30 kPa damage threshold, from 69 % under the *Moderate* scenario to 85 % under *Extreme*, reflects the larger release volumes under more severe snow loading. Even moderate-scenario avalanches on this corridor are typically destructive at road level.

Peak pressure also varies spatially (higher in the transit-zone upper corridor, lower but with greater deposit depths below), so protection objectives differ along the route: in the upper sector, dynamic impact loads are the primary concern for structural design; in the lower sector, deposit removal capacity and road-clearing logistics are the limiting operational factor. Km 155 (where 14 sub-paths of catchment A68 converge, with peak pressure regularly exceeding 100 kPa) is the single highest-priority section for structural protection, followed by km 110 and km 127–128. A segmented closure approach (standard practice in Switzerland and Austria (Rheinberger et al., 2009) but unreported for Chilean roads) is directly applicable to Route 115-CH. The corridor splits into operationally distinct segments:

- the lower corridor (km 98–117), largely shielded except for the localized hot-spots at km 105 and km 110, which require scenario-triggered closures or local protection while the remaining length stays open for local traffic;
- km 117–130 (the cluster of small-to-medium paths around Campanario and La Biblioteca), where scenario-triggered closures are coupled with structural protection on the highest-risk paths; and
- the upper corridor (km 138–159, including km 155), the highest-priority section, where structural protection (galleries, deflectors) would allow operations to continue during high-loading periods.

The intervening stretch around the Aduana complex (km 130–138) shows comparatively little simulated exposure. Implementing this segmented closure strategy would require extending current snow-monitoring practice and tying decision thresholds to the snow-depth scenarios used here. Completing a full individual-risk calculation (Wilhelm, 1998) will also require traffic data and avalanche occurrence probabilities; Hendrikx and Owens (2008) demonstrated for the Milford Road (New Zealand) that waiting-traffic risk can comprise 96–97 % of total collective risk on uncontrolled roads, with individual risk increasing by more than one order of magnitude when waiting traffic is accounted for. Rheinberger et al. (2009) further showed that hybrid mitigation strategies combining structural protection on short, high-risk sections with organizational closures elsewhere are more cost-effective than either approach alone. This hybrid framework is directly applicable to Route 115-CH, given its mix of concentrated hot-spots and extended low-exposure sections.

Route 115-CH is a principal overland trade corridor between Chile and Argentina, closed repeatedly each winter for snow and adverse-weather hazard (Subsecretaría del Interior, 2026). The high proportion of destructive crossings (77 % exceeding 30 kPa) at road level reinforces the case for targeted protection investment in the most exposed segments.

Ortner et al. (2023) applied RAMMS to large-scale avalanche hazard indication across the Gotthard corridor under multiple return-period scenarios. Their study and ours share the same corridor-scale approach (automated hazard indication combined with road-level exposure quantification), but differ in calibration depth (see Sect. 5.3).

https://doi.org/10.5194/egusphere-2026-3951
Preprint. Discussion started: 14 July 2026

A complementary approach is provided by Oberndorfer et al. (2026), who applied AvaFrame com1DFA to a single road section (B99 federal highway, Austrian Alps) with a probabilistic framework for the release condition: snow thickness and release-area extent were treated as random variables (beta-PERT distributions, Latin hypercube sampling), and 810 simulations per return period yielded probability maps of peak-pressure exceedance for standardized intensity classes. Their approach captured epistemic uncertainty in the initial condition while keeping SAMOS-AT friction at its defaults ($\mu = 0.155$, constant). Our work takes the complementary direction: a deterministic treatment of snow-depth scenarios (T10, T30, T100 from a national hazard study), but with friction calibrated by volume class from back-analysis.

Route 115-CH has a path density (208 paths over 61 km, 3.4 km^{-1}) comparable to the Rogers Pass section of the Trans-Canada Highway, where about 135 avalanche paths threaten a ∼40 km stretch (Stethem et al., 2003; Parks Canada, 2026). Rogers Pass operates under an active control program combining artillery triggering, forecast-based closures, and snowsheds; Route 115-CH currently relies on seasonal closure alone, with no active control or structural protection.

5.3 Limitations

Several limitations should be kept in mind when interpreting the results.

- Calibration coverage. The calibration anchors are two paths with markedly different elevation profiles: Campanario (release 2 515 m, road crossing 1 555 m, drop $H \approx 1000$ m) and La Biblioteca (release 2 011–2 129 m, road crossing 1 929 m, drop $H = 83$–193 m). Both paths sit within the km 125–130 stretch of the corridor, while the 208 simulated paths span release elevations from 1 055 to 3 200 m a.s.l. across the full 61 km. 78 % of paths (162 of 208) use $\mu = 0.20$ based on the single large-volume calibration event (Campanario 2011); the small-path calibration (La Biblioteca) yields $\mu = 0.30$–0.33 but does not constrain the large-volume regime. The Campanario 2022 validation event independently confirms $\mu \approx 0.20$ for this path (Sect. 4.1). A multivariate optimization approach (Fischer et al., 2015) should be pursued once sufficient data are available.

- Calibration cadastre. Ortner et al. (2023) drew on the Swiss avalanche cadastre, whereas our calibration is anchored on two paths. Expanding the calibration set across Andean corridors will require establishing a systematic event register, currently absent from Chilean practice.

- Model calibration range. The com1DFA module was originally tuned against documented avalanches with $V > 30\,000\ \mathrm{m}^3$ (Tonnel et al., 2023; Sampl and Granig, 2009). Several paths on Route 115-CH, particularly La Biblioteca ($V \approx 2\,800$–$3\,200\ \mathrm{m}^3$), fall well below this range. Our path-specific friction calibration partially compensates for this, but the model's intrinsic behavior at small volumes (turbulence parameterization, friction-regime transitions) remains less constrained.

- Peak pressure interpretation. com1DFA computes peak pressure from thickness-averaged flow variables ($p_{\mathrm{peak}} = \rho_0\, \bar{u}^2$), which does not account for local flow–obstacle interaction. Tonnel et al. (2023) note that wall-impact and run-up scenarios have not been systematically validated in com1DFA; Ortner et al. (2023) estimate ±50 % uncertainty in large-scale peak pressure estimates. Neuhauser et al. (2025) compared com1DFA particle velocities against in-flow sensor (AvaN-

https://doi.org/10.5194/egusphere-2026-3951
Preprint. Discussion started: 14 July 2026

ode) and radar data at the Nordkette test site and reported velocity root-mean-square errors of 5–10 % of maximum values for best-fit parameter sets, while also showing that narrow bands of friction parameters (μ, ξ, τ_0) yield similar deviations from observations, a manifestation of model equifinality that propagates into derived quantities such as peak pressure. More recently, Kohler et al. (2026) (in review) show that run-up height and the vertical extent of significant impact pressure on narrow obstacles are governed by distinct physical mechanisms (inertia-driven for run-up, velocity-independent for pressure height), and propose separate semi-empirical formulations for each within the Swiss guidelines framework. The peak pressures reported here are therefore order-of-magnitude indicators of intensity rather than precise engineering loads.

- DEM resolution. ALOS PALSAR (12.5 m native, bilinearly interpolated to 5 m) smooths terrain features that control flow routing. Miller et al. (2022) showed that coarser DEMs systematically overestimate runout distance while underestimating peak pressures. The net effect is a conservative bias for runout (overestimated, i.e. on the safe side for road exposure) but a potentially non-conservative bias for peak pressure at specific locations. Higher-resolution DEMs (e.g. LiDAR) would improve pressure estimates for structural design applications.

- Input uncertainty. Release areas and fracture depths from Dirección de Vialidad (2021) were digitized from PDF maps and verified against field photographs where available; the resulting bias towards more severe scenarios is likely deliberate and probably overstates exposure, which should be borne in mind when interpreting the estimates.

- Entrainment. Snow entrainment along the avalanche path is not modeled, although it can increase flow mass by a factor of 2–5 for large avalanches (Sovilla et al., 2006). The direction of the resulting bias is non-uniform: on long-runout paths, entrainment may extend the runout, while on short, steep paths it can increase deposition and reduce runout, so it cannot be characterized as uniformly conservative or non-conservative.

- Friction and density sensitivity. Under the *Severe* scenario, a $\pm 15\,\%$ perturbation of μ alters the number of road-reaching paths by $+6\,\%$ to $-13\,\%$ and mean peak pressure by $+16\,\%$ to $-9\,\%$; density variations (ρ_0 = 100–400 kg m^{-3}) scale peak pressure nearly linearly with ρ_0 but leave the road-reaching count essentially unchanged (Fig. 6). This follows from the model formulation: the driving stress and the dominant friction terms scale with density in the same way, so simulated velocities and runout are nearly insensitive to a constant ρ_0, while the derived pressure $p_{\mathrm{peak}} = \rho_0\,\bar{u}^2$ scales with it. The sub-minute arrival times hold across the tested parameter space, and the dominance of destructive-level pressures is robust to the friction perturbation; by the same linear scaling, however, the proportion of destructive-level crossings decreases substantially at the low-density bound ($\rho_0 = 100\,\mathrm{kg\,m^{-3}}$).

- Exposure, not annualized risk. All metrics reported here are conditional on avalanche release under the prescribed snow-loading scenarios: they describe where simulated avalanches reach the road and how hard they strike, but incorporate neither release probability nor traffic exposure. Proportions such as the 77 % of road crossings exceeding the vehicle-damage threshold therefore characterize crossings given an avalanche, not annual risk; converting them into individual or collective risk requires avalanche occurrence probabilities and traffic data (Wilhelm, 1998).

https://doi.org/10.5194/egusphere-2026-3951
Preprint. Discussion started: 14 July 2026

– Climate change. Warming is already altering avalanche regimes worldwide, with a documented shift towards wet-snow events and upward migration of starting zones (Eckert et al., 2024). While mean snow cover may decline, extreme snowfall episodes followed by rapid warming can maintain or increase avalanche magnitude, and high-end scenario projections of 4–5°C warming in the Chilean Andes (Vásquez et al., 2025) (SSP5-8.5) would raise the frequency of rain-on-snow and thermal-trigger events at higher altitudes. A higher snowline implies fewer events at low elevations but more at higher ones. This elevational shift matches the compound-event mechanism (heavy snowfall followed by rapid warming) documented for the La Biblioteca events in this study (Sect. 3.3). Open-source numerical frameworks (e.g. AvaFrame com1DFA, RAMMS, r.avaflow) are well suited to such climate-scenario analyses; the simulation database developed here provides the foundation for future work in this direction, following approaches such as those of Ortner et al. (2025).

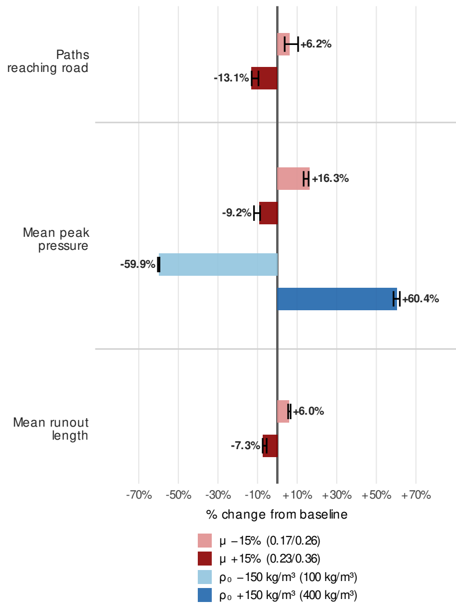

Figure 6. Sensitivity of corridor-scale exposure metrics to friction ($\mu \pm 15\,\%$) and release density ($\rho_0 \pm 150\,\mathrm{kg\,m^{-3}}$), as percentage change from the baseline under the *Severe* scenario (whiskers span the T10–T100 range). Metrics: path count, mean peak pressure, mean runout.

5.4 Transferability to other Andean corridors

The approach transfers directly to other Andean mountain roads where georeferenced release areas, a public DEM, and at least one calibration event are available. Routes of comparable exposure include Ruta 60-CH (Libertadores Pass), the busiest cross-Andean crossing; Ruta 7 (Carretera Austral, Aysén), where several sections traverse avalanche-prone valleys; and mining access roads in the Atacama and Coquimbo regions. The open-source AvaFrame platform (Oesterle et al., 2024), combined with the friction scaling derived here, lets other groups replicate the workflow at modest computational cost. Local back-analysis

https://doi.org/10.5194/egusphere-2026-3951
Preprint. Discussion started: 14 July 2026

calibration, even from few events, is preferable to the direct application of Alpine default parameters (e.g. the Swiss guideline values embedded in RAMMS or the SAMOS-AT presets), because these were calibrated against documented avalanches in the European Alps (Sect. 3.4) under snow and terrain conditions that may differ substantially from the semi-arid Andes. However, the absence of a systematic avalanche event register in Chile, comparable to the multi-decadal databases maintained in Switzerland, Austria, and France, limits the number of calibration cases and prevents the reliable statistical estimation of friction parameter distributions that European practice affords. Establishing such a register, beginning with the operational records already held by mining companies and *Dirección de Vialidad*, is therefore a prerequisite for expanding this approach across the Andes. The recent application of r.avaflow to the Parraguirre ice-rock avalanche in central Chile (Fürst et al., 2025) further shows the growing viability of open-source mass-movement modeling in the region.

6 Conclusions

We present a calibrated avalanche intensity map and quantitative road exposure assessment covering the entire 61 km of International Route 115-CH (Pehuenche Pass, ∼36° S, Maule Region, Chile), using the com1DFA module of the open-source AvaFrame framework. The assessment evaluates three snow-depth scenarios (*Moderate*, $T_{\mathrm{HS}} = 10$ yr; *Severe*, 30 yr; *Extreme*, 100 yr), based on the return period of three-day new-snow accumulation. The main findings are:

1. Back-analysis of four documented events on two paths, each providing a calibration/validation pair, yields Coulomb friction coefficients consistent with volume-dependent friction patterns and comparable to previous Chilean studies ($\mu = 0.18$–0.22 for large paths, $\mu = 0.30$–0.33 for small paths).

2. Of the 61 km of Route 115-CH, the road length physically reached grows from 19.6 km (32 %) under *Moderate* to 24.7 km (40 %) under *Extreme*. Up to 14 sub-paths of a single catchment (A68) converge on one kilometer (km 155), while km 110 gathers 11 sub-paths from three distinct catchments. Six primary hot-spot segments (km 105, 110, 122, 125, 127–128, 155) concentrate the greatest number of converging sub-paths and warrant priority risk-reduction investment.

3. Median peak pressures at road crossings increase from 61 kPa under *Moderate* to 104 kPa under *Extreme*, with maxima reaching 348–477 kPa. Of all simulated crossings, 77 % exceed the 30 kPa vehicle-damage threshold and 41 % exceed 100 kPa, implying that the large majority of avalanches reaching road level carry destructive pressures. Simulated arrival times (median 25 s, range 0–145 s) show that 83 % of road crossings occur within 60 s of release, leaving insufficient time for warning-based evacuation and requiring structural measures or preventive closures. The existing design assessment did not characterize arrival times corridor-wide.

4. The source-zone counts and peak pressure profiles provide a quantitative basis for route management: they support segmented closure protocols, structural-protection prioritization and targeted sensor deployment, measures applied in the European Alps but absent from Chilean practice.

5. A sensitivity analysis comprising 2 496 additional simulations indicates that, under the *Severe* scenario, the exposure estimates are robust to the tested parameter uncertainty: a $\pm 15\,\%$ friction perturbation changes road-reaching path counts by $+6\,\%$ to $-13\,\%$ and mean peak pressure by $+16\,\%$ to $-9\,\%$, while density variations ($\rho_0 = 100$–$400\,\mathrm{kg\,m^{-3}}$) scale pressure nearly linearly without altering runout (Fig. 6).

Priority recommendations for Route 115-CH: (i) establish an avalanche observation and reporting protocol to expand the calibration event database; (ii) obtain annual average daily traffic and vehicle speed data from *Dirección de Vialidad* to complete the individual-risk calculation; (iii) evaluate structural protection for km 155 (gallery or earthfill barrier) given the convergence of 14 sub-paths from catchment A68 and destructive-level pressures; and (iv) adopt a segmented closure protocol differentiating high-exposure sections from those with no simulated exposure.

The methodology is transferable to other Andean road corridors (e.g. Ruta 60-CH, Carretera Austral) using AvaFrame and publicly available data. More broadly, Chile lacks both a systematic avalanche event register and instrumented test sites comparable to those in Europe. International collaboration to establish such infrastructure would strengthen avalanche science across the Andes.

Outlook. Combining the deterministic snow-depth approach adopted here with a probabilistic release-volume distribution and volume-dependent calibrated friction (Oberndorfer et al., 2026) is a natural next step for Route 115-CH, and would couple epistemic uncertainty in release conditions with calibrated flow dynamics at the corridor scale.

Code and data availability. AvaFrame is open-source software available at https://avaframe.org/ and archived on Zenodo (Oesterle et al., 2024). The digitized release area database for Route 115-CH and supporting information from this study are openly available under a CC BY 4.0 license at https://github.com/OpenNHM/Route115Avalanches and archived on Zenodo (Latorre, 2026). Landsat 5 imagery was obtained from the USGS Earth Explorer (https://earthexplorer.usgs.gov/). The ALOS PALSAR DEM is publicly available from the Alaska Satellite Facility (https://search.asf.alaska.edu/).

Author contributions. IL designed the study, compiled and georeferenced the input data, performed all numerical simulations, carried out the road exposure and runout analyses, produced the figures, and wrote the original manuscript. MS and FO supervised the research and contributed to the interpretation of the results and to revising the manuscript.

Competing interests. Felix Oesterle is one of the developers of the open-source AvaFrame simulation framework used in this study. The authors declare that no other competing interests are present.

Acknowledgements. The authors thank the *Dirección de Vialidad* (MOP) for providing access to avalanche study data, and the CARASUR and Viento Puelche nivology teams of the ENEL Los Cóndores project for field records and observations. The numerical simulations were performed on the high-performance computing cluster at the Instituto Nacional de Hidráulica.

Financial support. No specific funding was received for this research.

https://doi.org/10.5194/egusphere-2026-3951
Preprint. Discussion started: 14 July 2026

References

Ancey, C.: Monte Carlo calibration of avalanches described as Coulomb fluid flows, Philos. T. Roy. Soc. A, 363, 1529–1550, https://doi.org/10.1098/rsta.2005.1593, 2005.

Barbolini, M., Gruber, U., Keylock, C. J., Naaim, M., and Savi, F.: Application of statistical and hydraulic-continuum dense-snow avalanche models to five real European sites, Cold Reg. Sci. Technol., 31, 133–149, https://doi.org/10.1016/S0165-232X(00)00008-2, 2000.

Barbolini, M. and Savi, F.: Estimate of uncertainties in avalanche hazard mapping, Ann. Glaciol., 32, 299–305, https://doi.org/10.3189/172756401781819373, 2001.

Bartelt, P., Salm, B., and Gruber, U.: Calculating dense-snow avalanche runout using a Voellmy-fluid model with active/passive longitudinal straining, J. Glaciol., 45, 242–254, https://doi.org/10.3189/002214399793377301, 1999.

Becerra Baeza, C. and de Rurange Espinoza, J.: Modelo de susceptibilidad a procesos de remociones en masa en rutas cordilleranas de Chile Central: Ruta 115 CH, Paso Pehuenche, Región del Maule, Investig. Geogr., 55, 89–110, https://doi.org/10.5354/0719-5370.2018.50799, 2018.

Bertrand, D., Naaim, M., and Brun, M.: Physical vulnerability of reinforced concrete buildings impacted by snow avalanches, Nat. Hazards Earth Syst. Sci., 10, 1531–1545, https://doi.org/10.5194/nhess-10-1531-2010, 2010.

Bründl, M., Etter, H.-J., Steiniger, M., Klingler, Ch., Rhyner, J., and Ammann, W. J.: IFKIS – a basis for managing avalanche risk in settlements and on roads in Switzerland, Nat. Hazards Earth Syst. Sci., 4, 257–262, https://doi.org/10.5194/nhess-4-257-2004, 2004.

Bühler, Y., von Rickenbach, D., Stoffel, A., Margreth, S., Stoffel, L., and Christen, M.: Automated snow avalanche release area delineation – validation of existing algorithms and proposition of a new object-based approach for large-scale hazard indication mapping, Nat. Hazards Earth Syst. Sci., 18, 3235–3251, https://doi.org/10.5194/nhess-18-3235-2018, 2018.

Bühler, Y., Bebi, P., Christen, M., Margreth, S., Stoffel, L., Stoffel, A., Marty, C., Schmucki, G., Caviezel, A., Kühne, R., Wohlwend, S., and Bartelt, P.: Automated avalanche hazard indication mapping on a statewide scale, Nat. Hazards Earth Syst. Sci., 22, 1825–1843, https://doi.org/10.5194/nhess-22-1825-2022, 2022.

Bunting Labs: AI Vectorizer – QGIS Plugin for AI-assisted vectorization, v2.0, available at: https://buntinglabs.com/solutions/ai-vectorizer-qgis-plugin, last access: 15 January 2025, 2024.

Casteller, A., Villalba, R., Araneo, D., and Stöckli, V.: Reconstructing temporal patterns of snow avalanches at Lago del Desierto, southern Patagonian Andes, Cold Reg. Sci. Technol., 67, 68–78, https://doi.org/10.1016/j.coldregions.2011.02.001, 2011.

Casteller, A., Häfelfinger, T., Cortés, E., Podvin, K., Kulakowski, D., and Bebi, P.: Assessing the interaction between mountain forests and snow avalanches at Nevados de Chillán, Chile and its implications for ecosystem-based disaster risk reduction, Nat. Hazards Earth Syst. Sci., 18, 1173–1186, https://doi.org/10.5194/nhess-18-1173-2018, 2018.

Christen, M., Kowalski, J., and Bartelt, P.: RAMMS: Numerical simulation of dense snow avalanches in three-dimensional terrain, Cold Reg. Sci. Technol., 63, 1–14, https://doi.org/10.1016/j.coldregions.2010.04.005, 2010.

Dalmasso, M., Frigo, B., and Chiaia, B.: A comparative analysis of avalanche risk assessment for local mountain roads, Geosciences, 15, 172, https://doi.org/10.3390/geosciences15050172, 2025.

Dijkstra, E. W.: A note on two problems in connexion with graphs, Numer. Math., 1, 269–271, https://doi.org/10.1007/BF01386390, 1959.

Ministerio de Obras Públicas, Dirección de Vialidad: Estudio de sendas de avalanchas, flujos de detritos y otros, en la Ruta 115-CH, sector La Mina – Límite Fronterizo, Región del Maule (prepared by Intrat Consultores), 2014.

Ministerio de Obras Públicas, Dirección de Vialidad: Estudio de ingeniería de detalle mejoramiento estabilización de taludes Ruta 115-CH, sector La Mina – Límite Internacional, Región del Maule (prepared by Ingeniería Cuatro), 2021.

Eckert, N., Keylock, C. J., Bertrand, D., Parent, E., Faug, T., Favier, P., and Naaim, M.: Quantitative risk and optimal design approaches in the snow avalanche field: Review and extensions, Cold Reg. Sci. Technol., 79–80, 1–19, https://doi.org/10.1016/j.coldregions.2012.03.003, 2012.

Eckert, N., Corona, C., Giacona, F., Gaume, J., Mayer, S., van Herwijnen, A., Hagenmuller, P., and Stoffel, M.: Climate change impacts on snow avalanche activity and related risks, Nat. Rev. Earth Environ., 5, 369–389, https://doi.org/10.1038/s43017-024-00540-2, 2024.

Fischer, J. T.: A novel approach to evaluate and compare computational snow avalanche simulation, Nat. Hazards Earth Syst. Sci., 13, 1655–1667, https://doi.org/10.5194/nhess-13-1655-2013, 2013.

Fischer, J. T., Kofler, A., Fellin, W., Granig, M., and Kleemayr, K.: Multivariate parameter optimization for computational snow avalanche simulation, J. Glaciol., 61, 875–888, https://doi.org/10.3189/2015JoG14J168, 2015.

Fürst, J. J., Farías-Barahona, D., Bruckner, T., Scaff, L., Mergili, M., Montserrat, S., and Peña, H.: The Parraguirre ice-rock avalanche 1987, semi-arid Andes, Chile – a holistic revision, Nat. Hazards Earth Syst. Sci., 25, 3559–3579, https://doi.org/10.5194/nhess-25-3559-2025, 2025.

Gauer, P., Kronholm, K., Lied, K., Kristensen, K., and Bakkehøi, S.: Can we learn more from the data underlying the statistical α–β model with respect to the dynamical behavior of avalanches?, Cold Reg. Sci. Technol., 62, 42–54, https://doi.org/10.1016/j.coldregions.2010.02.001, 2010.

Gauthier, F., Laliberté, J., and Meloche, F.: Assessing the predictive capability of several machine learning algorithms to forecast snow avalanches using numerical weather prediction model in eastern Canada, Nat. Hazards Earth Syst. Sci., 25, 5033–5053, https://doi.org/10.5194/nhess-25-5033-2025, 2025.

Glaus, J., Wikstrom Jones, K., Bartelt, P., Christen, M., Stoffel, L., Gaume, J., and Bühler, Y.: Simulation of cold-powder snow avalanches considering daily snowpack and weather situations, Nat. Hazards Earth Syst. Sci., 25, 2399–2419, https://doi.org/10.5194/nhess-25-2399-2025, 2025.

Hall, D. K. and Riggs, G. A.: Normalized-Difference Snow Index (NDSI), in: Encyclopedia of Snow, Ice and Glaciers, edited by: Singh, V. P., Singh, P., and Haritashya, U. K., Springer, 2011.

Hao, J., Zhang, X., Cui, P., Li, L., Wang, Y., Zhang, G., and Li, C.: Impacts of climate change on snow avalanche activity along a transportation corridor in the Tianshan Mountains, Int. J. Disaster Risk Sci., 14, 510–522, https://doi.org/10.1007/s13753-023-00475-0, 2023.

Hendrikx, J. and Owens, I.: Modified avalanche risk equations to account for waiting traffic on avalanche prone roads, Cold Reg. Sci. Technol., 51, 214–218, https://doi.org/10.1016/j.coldregions.2007.04.011, 2008.

Issler, D., Gisnås, K. G., Gauer, P., Glimsdal, S., Domaas, U., and Sverdrup-Thygeson, K.: Naksin – a New Approach to Snow Avalanche Hazard Indication Mapping in Norway, SSRN [preprint], https://doi.org/10.2139/ssrn.4530311, 2023.

Janeras, M., Oller, P., Arancibia, R., Pons, J., Costa, O., and Asensio, D.: Back-analysis modelling of the catastrophic avalanches in Sewell, Central Chilean Andes, in: Proc. International Snow Science Workshop, Grenoble–Chamonix Mont-Blanc, 2013.

Keylock, C. J. and Barbolini, M.: Snow avalanche impact pressure – vulnerability relations for use in risk assessment, Can. Geotech. J., 38, 227–238, https://doi.org/10.1139/t00-100, 2001.

Kohler, M. J., Gaume, J., Ancey, C., and Sovilla, B.: Distinguishing run-up height from pressure distribution during avalanche impact on narrow obstacles: mechanisms and semi-empirical prediction, EGUsphere [preprint], https://doi.org/10.5194/egusphere-2026-1181, in review, 2026.

Kristensen, K., Harbitz, C. B., and Harbitz, A.: Road traffic and avalanches – methods for risk evaluation and risk management, Surv. Geophys., 24, 603–616, https://doi.org/10.1023/B:GEOP.0000006085.10702.cf, 2003.

Latorre, I.: Route115Avalanches: avalanche exposure dataset for International Route 115-CH (Pehuenche Pass, Chile), Zenodo [data set], https://doi.org/10.5281/zenodo.20805729, 2026.

Leone, F., Colas, A., Garcin, Y., Eckert, N., Jomelli, V., and Gherardi, M.: The snow avalanches risk on Alpine roads network: Assessment of impacts and mapping of accessibility loss, J. Alpine Res., 102-4, https://doi.org/10.4000/rga.2501, 2014.

Margreth, S., Stoffel, L., and Wilhelm, C.: Winter opening of high alpine pass roads – analysis and case studies from the Swiss Alps, Cold Reg. Sci. Technol., 37, 467–482, https://doi.org/10.1016/S0165-232X(03)00085-5, 2003.

Martini, L., Baggio, T., and D'Agostino, V.: Comparison of two 2-D numerical models for snow avalanche simulation, Sci. Total Environ., 896, 165221, https://doi.org/10.1016/j.scitotenv.2023.165221, 2023.

McClung, D. M.: The effects of El Niño and La Niña on snow and avalanche patterns in British Columbia, Canada, and central Chile, J. Glaciol., 59, 783–792, https://doi.org/10.3189/2013JoG12J192, 2013.

Miller, A., Sirguey, P., Morris, S., Bartelt, P., Cullen, N., Redpath, T., Thompson, K., and Bühler, Y.: The impact of terrain model source and resolution on snow avalanche modeling, Nat. Hazards Earth Syst. Sci., 22, 2673–2701, https://doi.org/10.5194/nhess-22-2673-2022, 2022.

Naaim, M., Durand, Y., Eckert, N., and Chambon, G.: Dense avalanche friction coefficients: influence of physical properties of snow, J. Glaciol., 59, 771–782, https://doi.org/10.3189/2013JoG12J205, 2013.

Neuhauser, M., Köhler, A., Wirbel, A., Oesterle, F., Fellin, W., Gerstmayr, J., Dressler, F., and Fischer, J. T.: Particle and front tracking in experimental and computational avalanche dynamics, Nat. Hazards Earth Syst. Sci., 25, 4185–4202, https://doi.org/10.5194/nhess-25-4185-2025, 2025.

Oberndorfer, S., Sander, P., and Fuchs, S.: Multi-hazard risk assessment for roads: probabilistic versus deterministic approaches, Nat. Hazards Earth Syst. Sci., 20, 3135–3160, https://doi.org/10.5194/nhess-20-3135-2020, 2020.

Oberndorfer, S., Fischer, J. T., and Fuchs, S.: Quantifying the influence of avalanche release volume on runout probability: A case study of a mountain road section, Cold Reg. Sci. Technol., 242, 104734, https://doi.org/10.1016/j.coldregions.2025.104734, 2026.

Oesterle, F., Tonnel, M., Wirbel, A., and Fischer, J. T.: avaframe/AvaFrame (v1.8), Zenodo [code], https://doi.org/10.5281/zenodo.10664598, 2024.

Ortner, G., Bründl, M., Kropf, C. M., Röösli, T., Bühler, Y., and Bresch, D. N.: Large-scale risk assessment on snow avalanche hazard in alpine regions, Nat. Hazards Earth Syst. Sci., 23, 2089–2110, https://doi.org/10.5194/nhess-23-2089-2023, 2023.

Ortner, G., Michel, A., Kropf, C. M., Bründl, M., and Bresch, D. N.: Assessing the impacts of climate change on snow avalanche-induced risk in alpine regions, Nat. Hazards, 121, 10877–10904, https://doi.org/10.1007/s11069-025-07229-9, 2025.

Parks Canada: Highway avalanche control program, available at: https://parks.canada.ca/pn-np/mtn/securiteenmontagne-mountainsafety/avalanche/routes-highways, last access: 10 June 2026, 2026.

Ramírez C., L. and Mery G., J. P.: Las avalanchas en Chile: efectos y sistemas de control, Rev. Construcción, 6, 48–63, 2007.

Rauld, R., Fock, A., García-Huidobro, F., Letelier, V., Badilla, P., Gajardo, J., Luca, R., Muñoz, L., and Cancino, O.: Estudio de peligro, susceptibilidad, vulnerabilidad y medidas de mitigación en la ruta de alta montaña 115-CH, Paso Internacional Pehuenche, Región del Maule, in: Proc. XIV Congreso Geológico Chileno, La Serena, 2015.

Rheinberger, C. M., Bründl, M., and Rhyner, J.: Dealing with the White Death: Avalanche Risk Management for Traffic Routes, Risk Analysis, 29, 76–94, https://doi.org/10.1111/j.1539-6924.2008.01127.x, 2009.

https://doi.org/10.5194/egusphere-2026-3951
Preprint. Discussion started: 14 July 2026

Salm, B., Burkard, A., and Gubler, H. U.: Berechnung von Fließlawinen – Eine Anleitung für Praktiker mit Beispielen, Mitteilungen des Eidgenössischen Instituts für Schnee- und Lawinenforschung, Nr. 47, SLF, Davos, 1990.

Sampl, P.: SamosAT Modelltheorie und Numerik, Technical Report, AVL List GmbH, 2007.

Sampl, P. and Granig, M.: Avalanche Simulation with SAMOS-AT, in: Proc. International Snow Science Workshop, Davos, 2009.

Schaefer, M., Bugnion, L., Kern, M., and Bartelt, P.: Position dependent velocity profiles in granular avalanches, Granul. Matter, 12, 327–336, https://doi.org/10.1007/s10035-010-0179-6, 2010.

Schaerer, P.: The avalanche-hazard index, Ann. Glaciol., 13, 241–247, https://doi.org/10.3189/S0260305500007977, 1989.

Schweizer, J., Kronholm, K., Jamieson, J. B., and Birkeland, K. W.: Review of spatial variability of snowpack properties and its importance for avalanche formation, Cold Reg. Sci. Technol., 51, 253–272, https://doi.org/10.1016/j.coldregions.2007.04.009, 2008.

Sinickas, A., Jamieson, B., and Maes, M. A.: Snow avalanches in western Canada: investigating change in occurrence rates and implications for risk assessment and mitigation, Struct. Infrastruct. Eng., 12, 490–498, https://doi.org/10.1080/15732479.2015.1020495, 2016.

Sovilla, B., Burlando, P., and Bartelt, P.: Field experiments and numerical modeling of mass entrainment in snow avalanches, J. Geophys. Res., 111, F03007, https://doi.org/10.1029/2005JF000391, 2006.

Sovilla, B., Schaer, M., Kern, M., and Bartelt, P.: Impact pressures and flow regimes in dense snow avalanches observed at the Vallée de la Sionne test site, J. Geophys. Res., 113, F01010, https://doi.org/10.1029/2006JF000688, 2008.

Stethem, C., Jamieson, B., Schaerer, P., Liverman, D., Germain, D., and Walker, S.: Snow avalanche hazard in Canada – a review, Nat. Hazards, 28, 487–515, https://doi.org/10.1023/A:1022998512227, 2003.

Subsecretaría de Relaciones Económicas Internacionales: Comercio bilateral Chile–Argentina 2024, Technical Report, Ministerio de Relaciones Exteriores, Santiago, Chile, 2024.

Subsecretaría del Interior: Estadísticas de cierre del Paso Internacional Pehuenche (Ruta 115-CH), 2023–2026, response to access-to-information request No. AB001T0018565 (ORD. No. 14.830), certified by the coordinator of the Pehuenche border complex, with 35 Resoluciones Exentas of the Delegación Presidencial Regional del Maule, Ministerio del Interior y Seguridad Pública, Chile, 2026.

Sykes, J., Haegeli, P., and Bühler, Y.: Automated snow avalanche release area delineation in data-sparse, remote, and forested regions, Nat. Hazards Earth Syst. Sci., 22, 3247–3270, https://doi.org/10.5194/nhess-22-3247-2022, 2022.

Tonnel, M., Wirbel, A., Oesterle, F., and Fischer, J. T.: AvaFrame com1DFA (v1.3): a thickness-integrated computational avalanche module – theory, numerics, and testing, Geosci. Model Dev., 16, 7013–7035, https://doi.org/10.5194/gmd-16-7013-2023, 2023.

Vásquez, N. A., Mendoza, P. A., Lagos-Zúniga, M., Scaff, L., Muñoz-Castro, E., and Vargas, X.: Robust spatial changes in climate classes: insights from bias-corrected CMIP6 models across Chile, Environ. Res. Lett., 20, 014061, https://doi.org/10.1088/1748-9326/ad9d5b, 2025.

Vera Valero, C., Wever, N., Bühler, Y., Stoffel, L., Margreth, S., and Bartelt, P.: Modelling wet snow avalanche runout to assess road safety at a high-altitude mine in the central Andes, Nat. Hazards Earth Syst. Sci., 16, 2303–2323, https://doi.org/10.5194/nhess-16-2303-2016, 2016.

Vera Valero, C., Wever, N., Christen, M., and Bartelt, P.: Modeling the influence of snow cover temperature and water content on wet-snow avalanche runout, Nat. Hazards Earth Syst. Sci., 18, 869–887, https://doi.org/10.5194/nhess-18-869-2018, 2018.

Vergara, I., Moreiras, S. M., Araneo, D., and Garreaud, R.: Geo-climatic hazards in the eastern subtropical Andes: distribution, climate drivers and trends, Nat. Hazards Earth Syst. Sci., 20, 1353–1367, https://doi.org/10.5194/nhess-20-1353-2020, 2020.

Viento Puelche Expediciones: Nivología Los Cóndores 2018, Technical Report, 2018.

Viento Puelche Expediciones: Reporte especial de avalanchas 2 de julio de 2022 – Nivología Los Cóndores, Technical Report, 2022.

https://doi.org/10.5194/egusphere-2026-3951
Preprint. Discussion started: 14 July 2026

Voellmy, A.: Über die Zerstörungskraft von Lawinen, Schweiz. Bauztg., 73, 159–162, 212–217, 246–249, 280–285, 1955.

Wastl, M., Stötter, J., and Kleindienst, H.: Avalanche risk assessment for mountain roads: a case study from Iceland, Nat. Hazards, 56, 465–480, https://doi.org/10.1007/s11069-010-9703-6, 2011.

Wilhelm, C.: Quantitative risk analysis for evaluation of avalanche protection projects, in: Proc. Norwegian Geotechnical Institute Publication, 203, 288–293, 1998.

Zischg, A., Fuchs, S., Keiler, M., and Stötter, J.: Temporal variability of damage potential on roads as a conceptual contribution towards a short-term avalanche risk simulation, Nat. Hazards Earth Syst. Sci., 5, 235–242, https://doi.org/10.5194/nhess-5-235-2005, 2005.